



ASME Accepted Manuscript Repository

Institutional Repository Cover Sheet

First

Last

ASME Paper Title: A New Asperity-Scale Mechanistic Model of Tribocorrosive Wear: Synergistic Effects of Mechanical Wear and Corrosion

Authors: [Ali Ghanbarzadeh](#), [Farnaz Motamen Salehi](#), [Michael Bryant](#) and [Anne Neville](#)

ASME Journal Title: Journal of Tribology

Volume/Issue _____ 141(2) _____ Date of Publication (VOR* Online) _____ 11/10/2018 _____

ASME Digital Collection URL: <http://tribology.asmedigitalcollection.asme.org/article.aspx?articleid=2698528>

DOI: <http://doi.org/10.1115/1.4041246>

*VOR (version of record)

A New Asperity-Scale Mechanistic Model of Tribocorrosive Wear: Synergistic Effects of Mechanical Wear and Corrosion

Ali Ghanbarzadeh, Farnaz Motamen Salehi, Michael Bryant, Anne Neville

University of Leeds, School of Mechanical Engineering, Institute of Functional Surfaces, Leeds, UK

Corresponding author:

E-mail address: [*a.ghanbarzadeh@leeds.ac.uk](mailto:a.ghanbarzadeh@leeds.ac.uk) (Ali Ghanbarzadeh)

Abstract

A corrosive wear model is considered at the asperity-scale of a tribocorrosive wear system as well as the traditional Archard-type mechanical wear model. The geometry of the surface asperities are modified in a contact mechanics model with respect to both corrosive and mechanical wear calculations. This model was presented and validated for prediction of the electrochemistry in the first part of this work. The material used in the experimental part of this work was CoCrMo plate (working electrode) and Si₃N₄ ball as the counter body in a reciprocating configuration. Experiments were conducted at loads of 5, 7.5 and 10N and the contributions of total mechanical wear and corrosion were measured. The model is then tuned to predict the chemical and mechanical components of the total wear of the system. The synergistic effect of corrosion on mechanical wear and mechanical wear on corrosion are modelled numerically in this work. The values are then used to explain different components of mechanistic tribocorrosive wear models present in the literature. This deterministic model, for the first time, calculates the corrosion-enhanced wear in a tribocorrosive wear environment and proposes that changes in the topography are responsible for this synergistic effect. The results show a linear dependence of the corrosion enhanced wear, wear enhanced corrosion and the pure mechanical wear on the applied load. Results also suggest that the wear enhanced corrosion has a significant contribution in the overall degradation of the material.

Key words: Tribocorrosion, Wear modelling, Electrochemistry, Surface roughness; Wear Synergism

1 Introduction

In a tribocorrosion condition, a complicated mode of material degradation occurs. Mechanical removal of the material happens as well as transfer of ions and corrosion. These complex phenomena of interlinked mechanical and corrosive wear lead to a fast degradation of the material. The degradation rate in this condition cannot simply be calculated as the summation of the pure mechanical wear in the absence of the corrosion and the corrosion in the absence of mechanical wear. This behaviour is widely reported in the literature as the synergistic effect of corrosion and mechanical wear [1]. These synergistic effects have been observed in abrasion, erosion and sliding conditions [2-6]. The synergistic effects have been modelled mechanistically [7] but there is no deterministic approach to calculate these effects in a tribosystem because of its high system-dependency.

Mischler et al. [8, 9] demonstrated that the corrosive wear rate of the passive metal is strongly dependant on the mechanical parameters and the loading conditions. They have used Hertzian contact parameters to calculate the real contact area and related it to the depassivation area of the wear track. Mechanical parameters such as material hardness and the load were included in the model and were implemented into Faraday's equation to account for the corrosive wear. The model was a good starting point to include mechanical factors in the tribocorrosive wear modelling in severe contacts but there were no detailed contact mechanics calculations that would enable deterministic evaluation of the real area of contact at the asperity scale. No dynamics of surface roughness movement and topography evolution was considered. The model had been employed in other studies by the authors to assess different materials and working conditions [10-12]. There are several possible phenomena that lead to the wear-enhanced corrosion of tribocorrosive wear systems including: local acidification, increased mass transport by high turbulence, lowering fatigue properties and galvanic effects between wear scar and outside wear track [1]. The other synergistic effect known as the corrosion-enhanced wear, is probably the least studied subject in the tribocorrosion area. Corrosion enhanced wear can be the result of different mechanisms such as removal of the work-hardened products on the surface due to corrosion, grain boundaries being attacked by corrosive agents, increasing the stress concentrations at pitting sites and stress corrosion cracking [1].

Electrochemistry is an important part of any tribocorrosion model, since corrosion contributes considerably in the overall material degradation. Jemmely et al. [13] developed a current transient model using high field conduction equation considering the growth of passive film.

They numerically solved the current transient in one loading stroke of a sliding experiment. Olsson et al. [14] developed a current transient model considering the anodic polarisation and the mathematical model was fitted into the experimental measurements of transient current density. The principles of the current transient models in the literature are similar as they all incorporate the Butler-Volmer equation.

The topography of surfaces plays an important role in the degradation of the materials in contact. The topography evolves in time based on different mechano-chemical phenomena [15]. A deterministic tribocorrosion model should include evolutions in the topography of surfaces due to the both mechanical and electrochemical effects. The topography evolution of surfaces directly influences the real area of contact between two surfaces by changing the load carrying capacity and the conformity of the surfaces. The real area of contact is the area of de-passivation of the surface asperities thus affecting both corrosion and mechanical wear. Despite the importance of the effect of asperities and the real area of contact on tribocorrosive wear, literature lacks studies on the deterministic modelling of contact mechanics and its effect on the tribocorrosive wear. In a recent work, Stachowiak et al. [16, 17] developed a multi-asperity contact mechanics model that can deterministically calculate the real area of contact and the corresponding current density. They have used the same model to develop wear maps for tribocorrosion conditions [18].

Recently, Ghanbarzadeh et al. [19] used an electrochemical current transient model at asperity scale using and coupled contact mechanics with well-established electrochemical models [14] and predicted the evolution of current density over time in a tribocorrosive wear environment. The model is able to capture the electrochemistry on the asperity-scale and predict the macro-scale current density in a simple tribocorrosion experiment. The model was validated against the experimental electrochemical measurements of a ball-on-plate tribocorrosion rig. Predicted current results corresponded well with the measurements of current density at three different loads.

In this paper, although the same coupled wear-corrosion model framework is used to numerically determine the synergistic effects of corrosion and mechanical wear in the tribocorrosive wear environment, the complete description of the model is given. The model uses two degradation mechanisms; corrosive and mechanical. Both material degradation mechanisms are applied on the asperity-scale. The model employs a local Archard's wear equation to account for the mechanical wear and the corrosive wear is calculated using

Faraday's law. The geometry of the rough surfaces are then modified with respect to both material degradation models. The model was calibrated and then results were validated using experiments of ball on plate on a bespoke tribometer. The experimental part of this study and the results are presented in Section 2. The whole tribocorrosion model and its numerical implementation is explained in Section 2.3. Model results such as current density prediction and the total wear are presented in Section 5. The synergistic effects of corrosion on mechanical wear and mechanical wear on corrosion are then calculated based on the methodology explained in Section 5.1.3. All components of the tribocorrosive wear are modelled at three different applied loads and results are presented in Section 5.2. Limitations of the current approach and a brief discussion is reported in Section 6.

2 Experimental methodology and results

2.1 Test rig, sample preparation and materials

A bespoke tribometer was used to investigate tribo-corrosion condition between Si_3N_4 ball (12 mm diameter and $R_a \sim 5$ nm) and a wrought Low Carbon (LC) CoCrMo plate (ϕ 25 x 6 mm, exposed surface area = 4.9 cm^2 and $R_a \sim 20$ nm) in Phosphate Buffered Saline (PBS) solution. CoCrMo alloys are widely used for Metal-on-Metal (MoM) hip replacements and these alloys are the subject of numerous tribocorrosion studies to find the real mechanism of their degradation. The microstructures of CoCrMo can be complex and inhomogeneous, particularly cast alloys. In this study LC CoCrMo was used to simplify this conditions without tending to single elements. The generation of third-body abrasive particles because of inhomogeneity of the microstructure has also been reported [20]. This alloy is used extensively for bearing material and its tribocorrosion properties are fairly well understood both in-vivo and in-vitro [20-22].

Si_3N_4 is known to have very good mechanical strength, corrosion resistance, thermal and chemical stability. They are used as protective coatings and there are several studies to investigate their performance in tribocorrosion conditions [23, 24]. The chemical composition of the CoCrMo plate is reported in Table 3. In order to evaluate the electrochemistry of samples, an electrochemical cell was connected to the tribometer. To capture the electrochemistry, a 3-electrode electrochemical cell was integrated into the tribometer, of which the tribo-couple was taken as the working electrode (WE). The schematics of the tribo-electrochemical setup is shown in Figure 1.

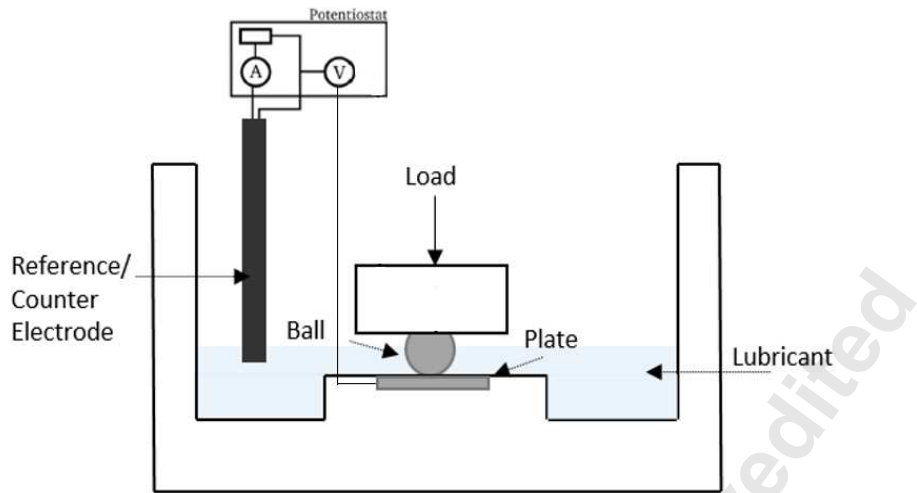


Figure 1 Schematic of tribometer and the three-electrode cell used for electrochemical measurement

Before the experiments, all CoCrMo plates were polished using automated polishing machine. At the final stage of polishing a diamond suspension of 3 μm was used to obtain an average surface roughness of 20nm. All samples were then cleaned by acetone before the experiments. Table 1 indicates the detail of sample properties used in the experiments. Table 2 shows the test condition used in this study. Tests duration was 90 minutes, however the sliding condition was only for 30 minutes. Before and after the tests the samples were left in static condition for 30 minutes to stable the current transients. All experiments were repeated twice to ensure the repeatability of the results. Wear in a tribocorrosion condition can be affected by a whole range of physical, chemical and electrochemical parameters. Validating the current model for a whole range of parameters is cumbersome. However the range selected in this study was chosen to be close to the hip simulator loading conditions [25, 26]. The experimental results of this paper only aim at validating the developed numerical model and its calibration. In addition, a more comprehensive parametric study to investigate the effect of important physical, mechanical and electrochemical parameters on tribocorrosive wear is being undertaken by the authors.

Table 1 Properties of the samples used in the experiments

Parameters	Si ₃ N ₄ ball	CoCrMo plate
R _q Roughness (nm)	5	20
Diameter (mm)	12	—
Elastic Modulus (GPa)	310	210
Hardness (GPa)	25	4.5

Table 2 Tribocorrosion test parameters used in this study

Load	5; 7.5; 10 N
Max Hertzian Pressure	0.79; 0.91; 1 GPa
Displacement Amplitude	5 mm
Sliding Speed	10 mm/sec
No. Cycles	1800 (1 ms dwell time)
Lubricant	PBS.

Table 3 Chemical composition of the CoCrMo plate

Chemical compositions (%wt)											
	C	Si	Mn	P	S	Cr	Fe	Mo	N	Ni	Co
CoCrMo plate	0.04	0.21	0.69	<0.005	0.0008	27.365	0.41	5.4	0.17	0.48	Bal.

2.1.1 Post-test surfaces analysis

After tribocorrosion tests, vertical scanning interferometry (VSI, NPFLEX, Bruker, AZ, USA) was used to analyse the wear of the surfaces of the steel plate samples. Surfaces were scanned and corrected to remove any surface form or tilt. In this study, the depth of the wear scar was measured at least in three different positions across the wear track.

Scanning Electron Microscope (SEM, EVO MA15, Zeiss Oberkochen, Germany) was utilised to enable visual examinations of the surfaces under high magnifications. All SEM images were taken from the plate samples in the centre of the wear tracks.

2.2 Experimental results

2.2.1 Electrochemistry

The current was measured in static conditions as well as in sliding conditions. There was a very small current flow during the static condition since the CoCrMo plate is not subjected to any mechanical wear. As soon as the sliding started, there was a significant shift in current. Figure 2 presents the current trend over time during sliding conditions under various loads. This increase in current can be related to the depassivation of protective film formed on the surface.

This depassivated area becomes a net anode, and the remaining surface which is of a large area becomes a net cathode.

As can be seen in Figure 2, the current increased further as the test progressed. The reason for this behaviour can be explained by changes in the topography of the surfaces and increase in the real area of contact.

Moreover, it can be observed that the current is higher when applying higher load (see Figure 2). This is to be expected since the increased contact pressure causes more severe asperity contact in the boundary lubrication regime, which leads to more severe abrasion of the passive film and hence an increased corrosion current.

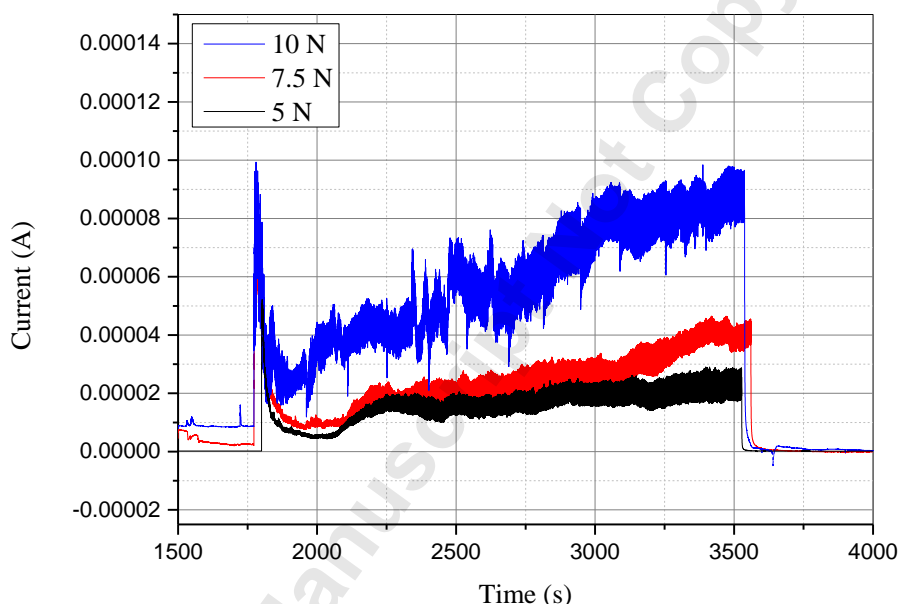


Figure 2 Evolution of the current density as a function of time for 3 applied loads of 5, 7.5 and 10 N

2.2.2 Wear measurements

After the tribological tests, the CoCrMo plates were rinsed with heptane and then analysed using NPFLEX (Bruker, AZ, USA) vertical scanning interferometry (VSI) to examine the surface wear scars. Surfaces were scanned and then the image obtained from the scan was filtered and corrected using the 'terms removal' function to remove any surface form or tilt. The average depth of the wear scar was measured in three different positions and appropriate results are presented at experimental mean \pm standard deviation. The wear on the ball was much lower than the wear on the plate (as expected) due to the difference in the material hardness and also the inert nature of the ball. General flattening of the Si_3N_4 ball was observed which was

negligible compared to the wear on the plate. Figure 3 shows typical images for wear scars on the plates for each loading condition. As can be seen with increased load, and thus increased contact area and pressure, the area of wear scars increased as a result of sliding. Moving from 5 N to 10 N the average wear scar depth increased from 1 to 3 μm (see Figure 4). From the results, it is clear that surfaces under higher applied load showed wider and deeper wear scar. This is due to the greater contact area and more asperities that are likely to come into contact and equally are more likely to shear and depassivate, resulting in higher corrosion currents as shown in Figure 2.

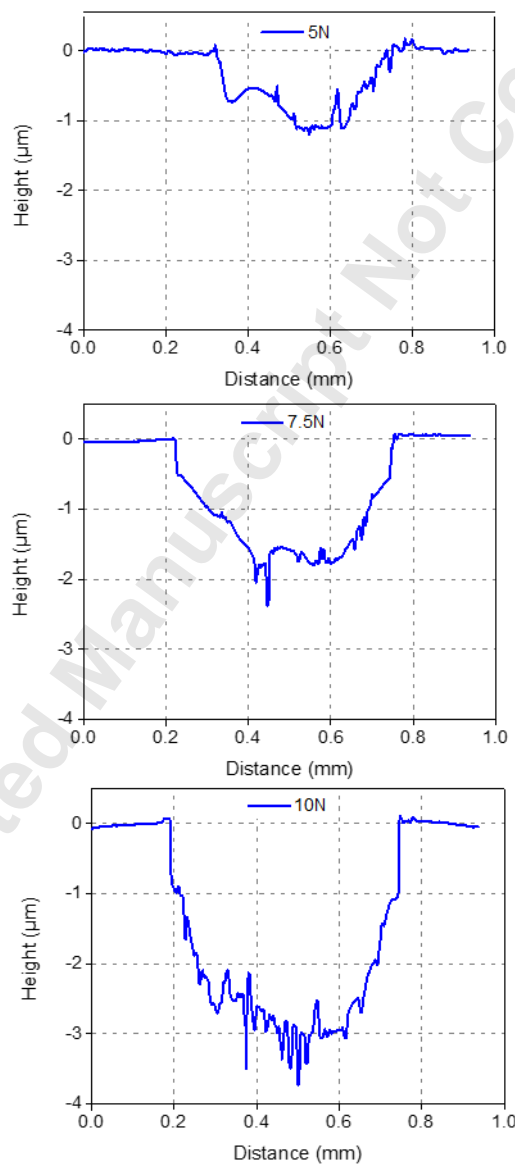


Figure 3 2D microscopic images of the plate wear scars after reciprocating tribometer testing under various loads of (a) 5N (b) 7.5N (c) 10N

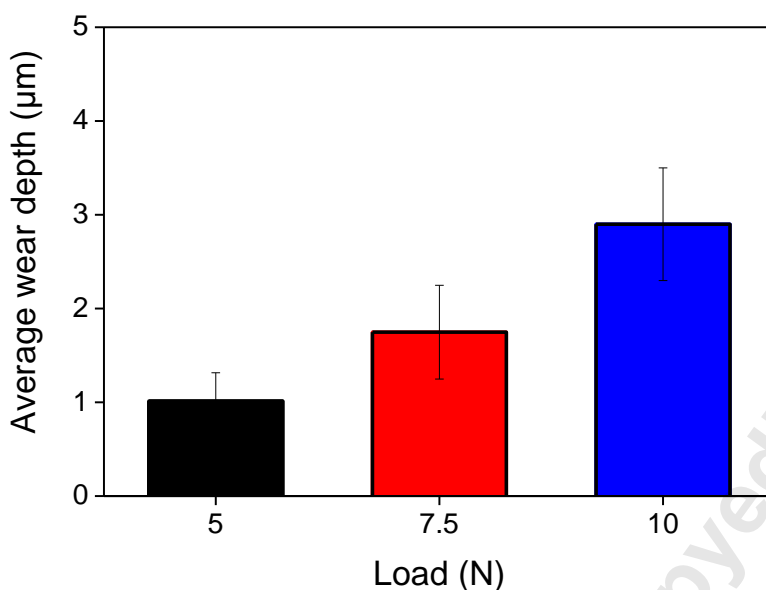


Figure 4 Wear scar depth for CoCrMo samples during reciprocating tribometer testing with varying load

3 Components of the model

The tribocorrosion model developed in this work considers the dynamic process of the degradation of material both mechanically and electrochemically. Contacting surfaces are rough and they move relative to each other. It is assumed that a thin layer of passive layer is protecting the entire surface from corrosion. Contact mechanics determine the contact of rough surfaces and the real area of contact and the corresponding stresses are calculated. It is assumed that the passive protective layer is removed when the direct asperity contacts occur [1, 8]. Hence, the passive protective layer is removed at the real area of contact spots. This is certainly a simplification since at some contacting point there might be partial disruption of the passive film or even no disruption. Movement of the surfaces results in the contact of new asperities. The schematic of the real area of contact and the movement of surfaces is shown in Figure 5. The contacting asperities with no passive layer on top, are exposed to the corrosive environment and the re-passivation of the oxide layer occurs. The immediate transfer of ions from the surface to re-form the oxide layer or dissolve in the solution increases the current density measurements. Rapid formation of the passive film on the surface then leads to the fast decrease in the current density. The model employs a local electrochemistry model to account for the current density variations and the corresponding material loss due to transfer of ions based on Faraday's law. It should be noted that the share of the current going to the oxide and

the share going into the solution is not considered in this work. This will be possible in the next iterations of the model as more physical and chemical parameters would be implemented.

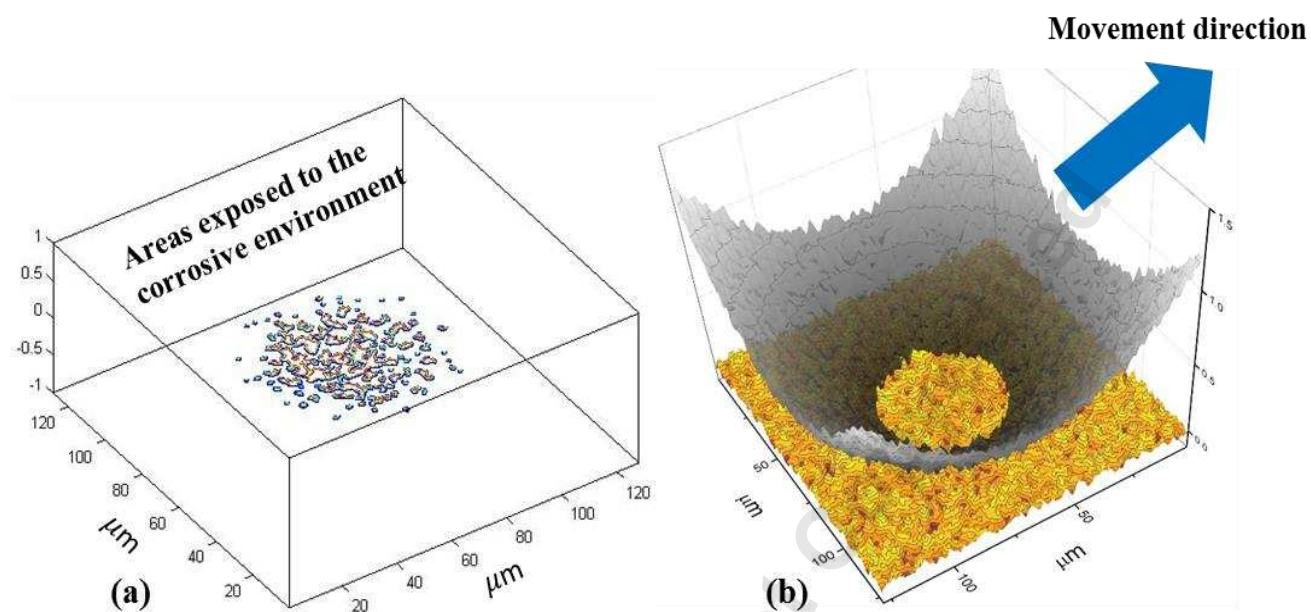


Figure 5 Movement of the surfaces and exposure of the nascent surface asperities to the corrosive environment

The geometry of the tribocorroded surface is then modified based on mechanical and the corrosive local wear. This procedure is continued until the time of the experiment is reached. The model is able to distinguish the mechanical and corrosive wear at any time instance and can capture their evolution in time. A flowchart of the numerical procedure has been shown in Figure 6. Individual components of the model are explained in this section.

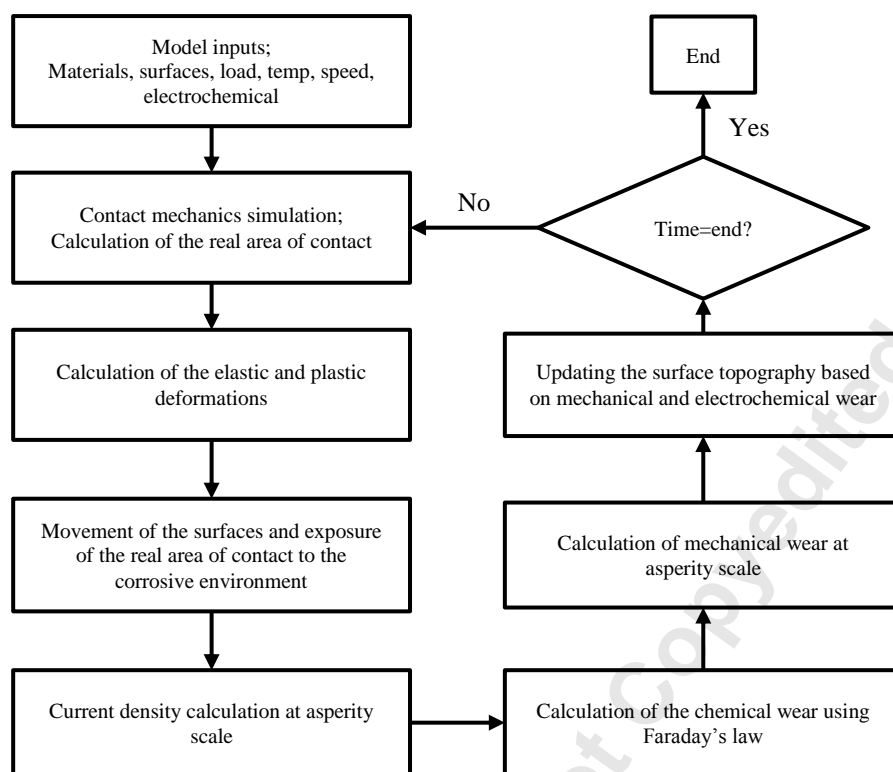


Figure 6 Flowchart of the whole numerical approach for calculation of the electrochemistry in tribocorrosion conditions

3.1 Contact mechanics

The contact mechanics model in this work incorporates the complementary potential energy concept [27] for calculating the real stress and strains using the following equation:

$$V^* = \frac{1}{2} \iint p \bar{u}_z dx dy - \iint p \bar{u}_z^* dx dy \quad (1)$$

where p is the contact pressure and V^* , \bar{u}_z and \bar{u}_z^* are complementary potential energy, surface deformation and prescribed displacement respectively.

The model is based on the Boundary Element Method (BEM) that only discretises the boundary of the contacting solids. Rough surfaces are the inputs of the contact mechanics simulation either from the direct measurement of real samples or by generating them with digital filters [28]. The model is presented in another work of the authors in Ref [29] for dissimilar materials in contact. The model is used to calculate the true contact areas as well as the contact pressures in normal direction and the normal displacements. The ability of the model to calculate the tangential tractions is not of the interest in this paper. The contact model is an elastic-perfectly plastic model, taking the hardness of the material as the plastic flow criteria. It is assumed that

the asperities reaching the hardness of the material will freely float on the surface and the plastic deformation can be simply calculated from the subtraction of the rigid body movement and the elastic deformation. A Discrete Convolution and Fast Fourier Transform (DC-FFT) model is also used for the numerical efficiency. The surfaces move relative to each other to simulate the sliding condition. This can be simply carried out by shifting the matrices containing the surface asperity height values in one direction.

3.2 Corrosive wear model

The corrosive wear model is based on Faraday's law and the calculation of the volume of the metal ions transferred to the surface and used to form the oxide. The formulation used for the corrosive wear is as the following:

$$V_c = \frac{QM}{nF\rho} \quad (2)$$

V_c is the volume of metal removed by anodic reactions. Q is the total electric charge passed and is calculated by integrating the current over the time ($Q = \int_0^t i dt$) when an over-potential is applied. M is the atomic mass for the metal, n is the charge for the oxidation reaction, ρ is the density of the passive metal and F is the Faraday constant. In a real tribocorrosive wear environment, the anodic and cathodic currents are always equal at the free corrosion potential (E_{corr}) and the measured anodic current in this condition will be the real I_{corr} and must be used as a representation of the contribution of the corrosion. Applying over-potentials on a sliding system will significantly alter the equilibrium condition so that the cathodic reaction becomes negligible and the measured current will be only the anodic current from the working electrode. Working in such conditions is different from a real natural tribocorrosion condition that occurs around the E_{corr} of the metal alloy. Applying an over-potential can change the PH of the surface and this can eventually have impact on the corrosion. Therefore, strictly speaking, the I_{corr} used in any tribocorrosion study of the metallic alloys to measure the contribution of all the mechanical and chemical components of the tribocorrosive wear should be determined at E_{corr} . Despite this, the majority of the studies in the tribocorrosion area apply over-potentials and shift the surfaces from their natural freely-corroding state. The models in the literature also incorporate potentiostatic conditions based on anodic polarisation. In this paper, the same concept has been considered but the development of a model for real corrosion conditions is the subject of ongoing works of the authors.

An important parameter to be considered in the electrochemical wear model of Equation 2 is the total electric charge (Q). Calculation of Q will be possible when the current passing through the passive film is successfully captured. Although the evolution of the current density results were validated against the current density measurements on a pin-on-plate tribometer in the previous work [19], the complete formulation is given here. The electrochemistry model is at asperity-scale and the corresponding current density is calculated considering the inhomogeneous nature of the surface asperities in a deterministic manner. The summation of the local current densities results in the calculation of the macro current density which is comparable with the experimental results. The model assumes a film growth model with an anodic polarization using a well-established electrochemical model by Olsson et al. [14] as the following:

$$i_{growth} = \frac{i_{growth}^0 \cdot e^{g^+ U}}{1 + g^+ \cdot E_0 \cdot k_{film} \cdot i_{growth} \cdot e^{g^+ U} \cdot t} \quad (3)$$

where i_{growth}^0 is the long-term growth current, k_{film} is the film growth kinetic rate, U is the over potential and $U = U_{app} - E_{corr}$, E_0 is the electric field inside the film, t is the time and g^+ is the generalised charge transfer factor formulated as:

$$g^+ = \frac{\alpha^+ F}{RT} \quad (4)$$

α^+ is the generalized charge transfer coefficient [30], F is the Faraday constant (96485.33289 (C/mol)), R is the ideal gas constant and T is the absolute temperature.

When the surfaces move and different number of asperities come into contact, these current profiles are superimposed on each other (because the macro current is the summation of all asperity currents). The superimposition of current profiles will lead to the current of a single stroke to fluctuate. The superimposition takes into account the depassivation kinetics as well as the speed of movement of the surfaces. The profiles of single asperity currents will be added to each other with time increments which is equal to $\frac{\Delta X}{V}$. where ΔX is the size of the nodes used for relative movements and V is the sliding velocity. The calibration of the current for one sliding stroke has been formulated and presented in Section 4.1.

3.3 Mechanical wear model

The current model employs a local form of the Archard wear equation for wear depth calculation. The local wear depth of each point at the surface is given by:

$$\Delta h(x, y) = \frac{K}{H} \cdot P(x, y) \cdot \Delta t \cdot v \quad (5)$$

in which H , K , P , v , and Δt are the material hardness, dimensionless Archard's wear coefficient, local contact pressure, sliding speed, and time step respectively [31]. It should be noted that Archard used wear volume in his equation. In order to use the Archard wear formula, the wear volume was divided by the area of the wear track. Although not uniform, but it gives a rough estimation of the wear depth. This method was used widely in the literature [31-33]. The contact conditions vary from the plate and the ball. The ball is constantly in contact and the positions of the contact on the plate is moving. Therefore numerical implementation of wear on the two surfaces should be different. The wear calculated from Equation 5 (using the hardness of the ball) is directly used to modify the geometry of the ball in each step. However, the wear on the plate is calculated in each time step using a modification factor. Since the wear of plate does not occur all the time, wear calculated from Equation 5 (using the hardness of the plate) is divided by the ratio of the length of the wear track to the nominal contact area to find the balance. These values of wear will be then deducted from the surface profiles and the surfaces are modified in every time step.

All the parameters in Equation 5 except K are calculated in the contact mechanics simulation. K is determined by the calibration of the model which is explained in detail in Section 4. The mechanical wear depth calculated from Equation 5 is used to locally modify the geometry of the surface based on the asperity pressure distribution. The total mechanical wear can be calculated by accumulating the mechanical wear at loading cycles. The value of the total mechanical wear is reported in Section 5.1.1 and its evolution in time is presented. The comparison of the mechanical and the corrosive wear is also reported.

4 Model calibration

Calibration of the model is necessary prior to testing its predicting capabilities. The calibration is conducted for two steps for the corrosive wear model explained in Section 3.2 and the mechanical wear model explained in Section 3.3. The calibration procedures for both steps are explained as the following.

4.1 Calibration of the current density

In each time step, the overall current is calculated through the real area of contact as the following:

$$A_i = N_i \cdot i_{growth}(t) = N_i \cdot \frac{i_{growth}^0 \cdot e^{g^+U}}{1 + g^+ \cdot E_0 \cdot k_{film} \cdot i_{growth}^0 \cdot e^{g^+U} \cdot t} \quad (6)$$

In which A_i is the total current in one loading step, N_i is the number of asperities in the contact in one loading (real area of contact) at i th time step. The current in one sliding stroke is then formulated as:

$$i_{stroke}(t) = N_0 \cdot i_{growth}(t - t_0) + N_1 \cdot i_{growth}(t - t_1) + N_2 \cdot i_{growth}(t - t_2) + \dots + N_i \cdot i_{growth}(t - t_i) + \dots + N_M \cdot i_{growth}(t - t_M) \quad (7)$$

$i_{stroke}(t)$ is the current density in a sliding strokes as a function of time, N_0, \dots, N_M are the number of asperities in contact calculated through the contact mechanics simulation considering the movement of surfaces in tangential direction. t_0, \dots, t_M are the time of each loading step when surfaces move relative to each other in one stroke and are calculated from:

$$t_i = (i) \cdot \frac{\Delta X}{V} \quad (8)$$

where ΔX is the size of the nodes used for relative movements and V is the sliding velocity and i is the number of the step. The only parameter for electrochemical model calibration is i_{growth}^0 which can be obtained from the experimental current measurements. The current of Equation 7 has been fitted to experimental results of current measurements only for one sliding stroke and the corresponding fitting parameter (i_{growth}^0) has been extracted. The averaged electrochemical response of three repeated experiments were used and fitted to obtain the calibration parameters.

The current density calibration process considers both depassivation and repassivation periods. The inhomogeneity of the surface asperity distributions results in the inhomogeneous contact of such asperities and therefore the current density in one sliding stroke shows a fluctuation over the time period. The calibration parameters has been reported in Table 4 and used throughout this paper for the rest of the simulations. It is known that such mechanistic numerical models are dependent on the accurate determination of the calibration parameters.

Therefore, a sensitivity analysis of the electrochemical fitting parameter (i_{growth}^0) is conducted and presented here. The values of i_{growth}^0 are varied from 10^{-10} to 10^{-19} and the results of the corrosion is plotted in Figure 7. The results suggest a great influence of i_{growth}^0 on the corrosion prediction of the model.

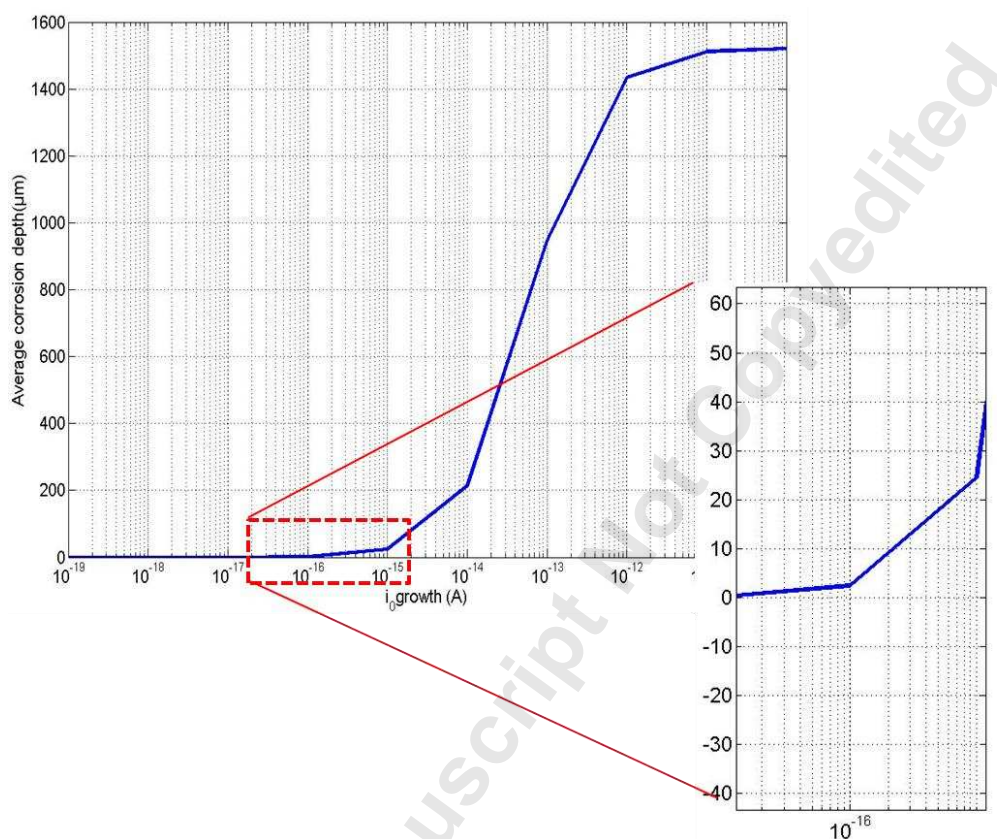


Figure 7 Sensitivity of the corrosion model to the calibration parameter (i_{growth}^0)

Table 4 Fitting parameters in the electrochemistry model

Fit parameters	Value
i_{growth}^0 ($A/\mu m^2$)	10^{-16}

4.2 Calibration of the mechanical wear

The experimental measured wear is the total volume of the material loss due to the effect of mechanical and the corrosive wear and their interactions. The share of any electrochemical material loss can be calculated by using the Faraday law incorporating the total charge and

integrating the current density over the time. Subtracting the value of total corrosive wear from the total experimental measured wear gives the total mechanical wear of the system.

It is important to note that mechanical wear is the summation of the pure mechanical wear and the corrosion enhanced wear. The total mechanical wear is used to calibrate the Archard wear equation. It is reasonable to take this approach since the mechanical wear calculated in the model (via equation 5) is the total mechanical wear of the system. The total calculated wear is affected by the surface topography evolution and the effect of corrosive wear is already considered in the topography evolution. There are some methods to measure the pure mechanical components by cathodic protection and to stop any charge transfer from the working electrode. However there are some debates if this method can completely turn off the effect of corrosion on the total wear due to different rates of hydrogen embrittlement into the materials that can induce cathodic wear [34, 35]. This method was not used in this work and another alternative of separating pure mechanical wear and the corrosion enhanced wear is introduced which is explained in detail in Section 5.1.3.

The experimental results for the applied load of 10 N has been used to calibrate the Archard equation and the corresponding K value (see Table 5) has been used for the all the other simulations. Similar to the electrochemical parameter, calibration of the mechanical wear is also influencing the accuracy of the predictions. For this reason, a sensitivity analysis of the K value is carried out. Both mechanical wear and the corrosion are calculated for K values ranging from 10^{-9} to 10^{-7} and the results are plotted in Figure 8. As expected, the mechanical wear and corrosion are both changing linearly with the coefficient of the mechanical wear.

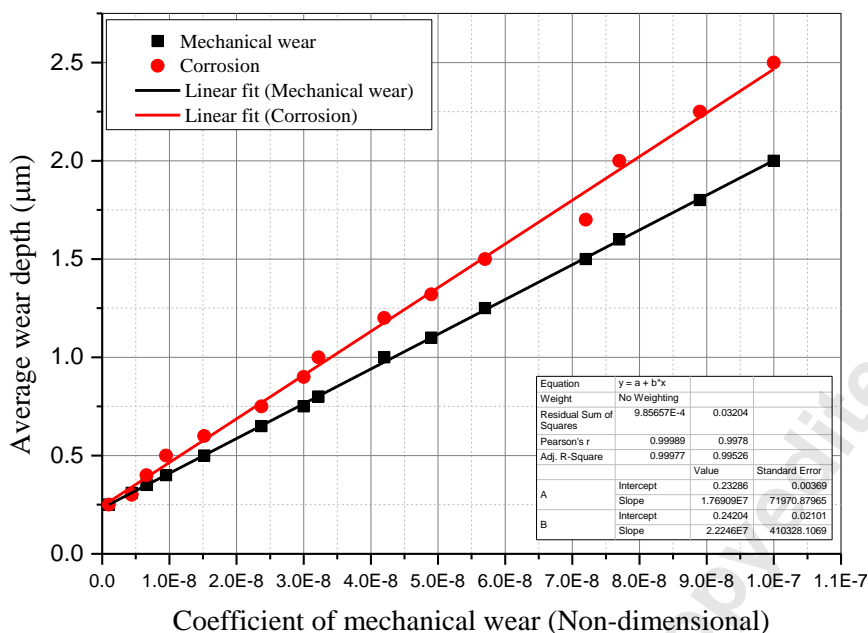


Figure 8 Sensitivity of the model to the non-dimensional coefficient of mechanical wear

Table 5 Calibrated dimensionless coefficient of mechanical wear

Parameter	Value
K (dimensionless)	7×10^{-8}

5 Model results and discussion

Once the model is calibrated, it can capture the evolution of the current density as a function of time. The mechanical and the corrosive wear can be calculated on the asperity-scale and the geometry of the surfaces are modified accordingly. The accumulative corrosive and the mechanical wear can be then calculated by the summation of each individual wear component on each asperity and the average corrosive, mechanical and the total wear depth of the surface can be modelled. It should be noted that the degradations mechanisms in reality for CoCrMo alloys are complex and non-uniform [20] and this non-uniformity can be promoted by the non-uniform microstructural properties of the material. This model, for the first time, presents an adaptable framework for the prediction of wear and corrosion (i.e. electrochemical current) where the physics and chemistry of the problem have been decoupled. The nature of the model and prediction of corrosion at the asperity and evolution of the surfaces due to material loss is, by its implementation, highly non-uniform, representing the observed phenomena. The area of passive and depassivated material within a tribological contact have been simulated which changes with time and evolving geometry.

5.1 Predicting the evolution of tribocorrosive wear and its components

5.1.1 Mechanical components of the total wear (V_{mech})

The total tribocorrosive wear of the system is the summation of the total corrosive and the total mechanical wear on the system. The total mechanical wear of the system can be calculated using the mechanical wear model explained in Section 3.3. The total mechanical wear is then calculated by accumulating the amount of material removed using Archard's wear model and the amount of plastic deformation on the surface asperities. The total mechanical wear depth evolution for applied loads of 5, 7.5 and 10 N are plotted in Figure 9. It should be noted that this mechanical wear is the total mechanical wear and contains the pure mechanical wear as well as the corrosion enhanced mechanical wear components. This is because the mechanical wear is being calculated while the topography is getting updated by mechanical and corrosive wear components. This means that the corrosion is affecting the behaviour of the tribosystem. To distinguish between the pure mechanical wear and the corrosion enhanced mechanical wear, a methodology is introduced in Section 5.1.3 and the results are presented.

Results of the total mechanical wear presented in Figure 9 suggest that there is a higher rate of wear at the start of the simulation which corresponds to the higher plastic deformation. The rate of mechanical wear then decreases gradually to get to a steady-value which can correspond to the steady-state wear rate observed in many tribological systems.

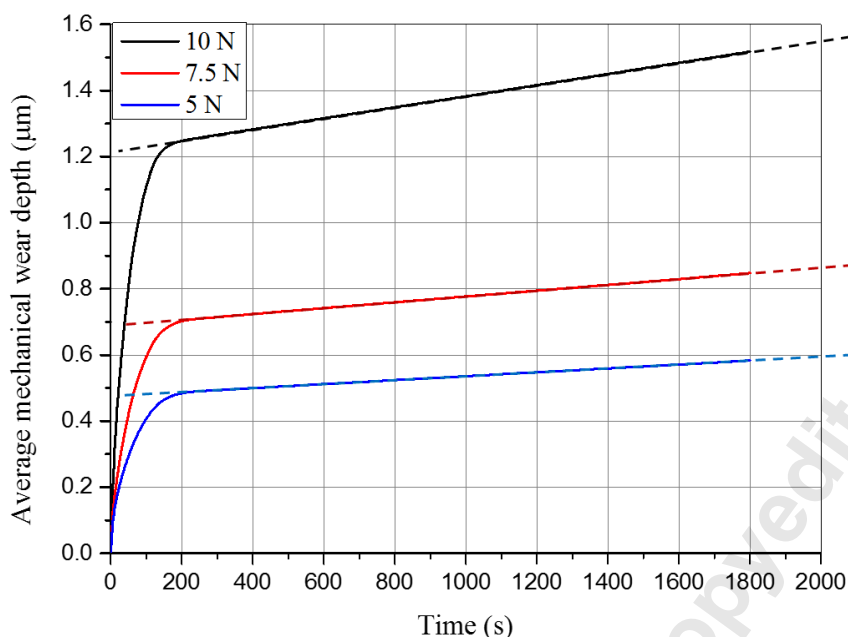


Figure 9 Average mechanical wear depth evolution for applied loads of 5, 7.5 and 10 N from simulations in tribocorrosion condition

5.1.2 Chemical component of total wear (V_{chem})

The amount of total corrosive wear can be calculated by accumulating the corrosive wear calculated at every loading cycle of the simulation by using Faraday's law. The corrosive wear is proportional to the real area of contact. The results for the evolution of the corrosive wear in time for applied loads of 5, 7.5 and 10 N h is plotted in Figure 10. Unlike the total mechanical wear, results of Figure 10 show an increase in wear rate as a function of time. This is due to the conformity of the surfaces in contact and the increase in the real area of contact hence increasing the number of the de-passivated asperities. This results are interestingly in line with the results of a recent experimental-analytical work [36] which reports a similar pattern in the real area of contact measured experimentally using a new set-up. It is also clear that the higher applied load results in the faster increase in the corrosive wear which can be attributed to the faster modification of the surface topography and the real area of contact.

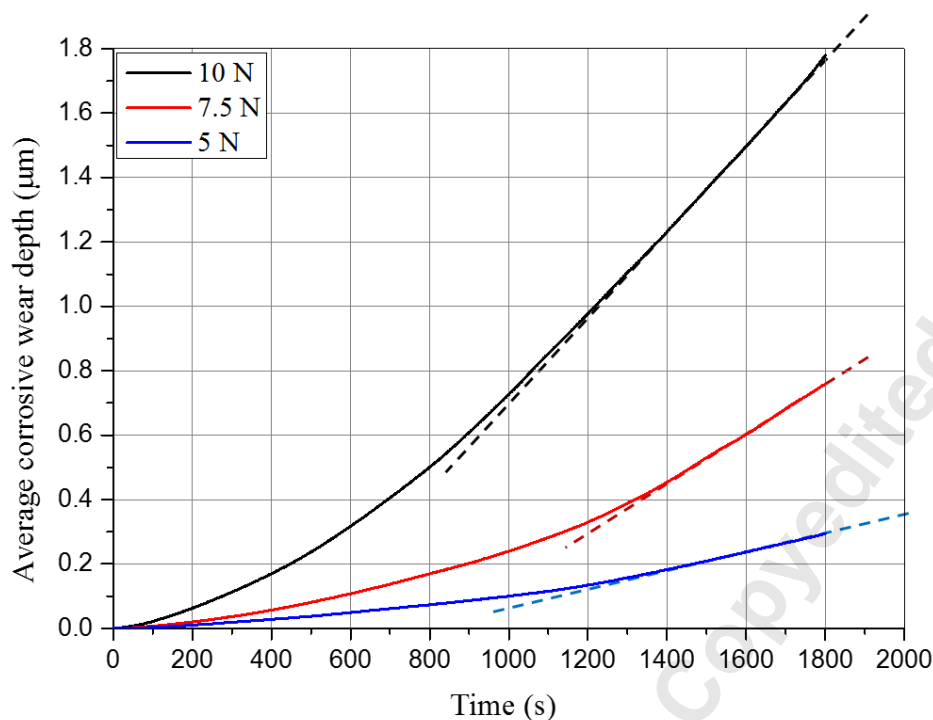


Figure 10 Average corrosive wear depth evolution for applied loads of 5, 7.5 and 10 N from simulation in tribocorrosion condition

Figure 11 shows the evolution of the total mechanical wear and the corrosive wear for the case of 10 N as well as the total tribocorrosive wear. It is interesting to see the patterns for the two degradation mechanisms in this case. The total mechanical wear has a higher rate at the beginning in comparison to the corrosive wear. The corrosive wear rate tends to increase unlike the mechanical wear rate which decreases as a function of time. Eventually, the total corrosive wear becomes more than the total mechanical wear. These wear patterns and the comparison between them can give insight into the degradation mechanisms of the materials in a tribocorrosive wear environment and are useful for designers to optimise the systems to achieve the desired performance.

The components of total mechanical wear and the total corrosive wear at the end of the simulations have been plotted together in Figure 12 as well as the measured experimental values. The share of total mechanical and corrosive wear can be clearly seen in the figure.

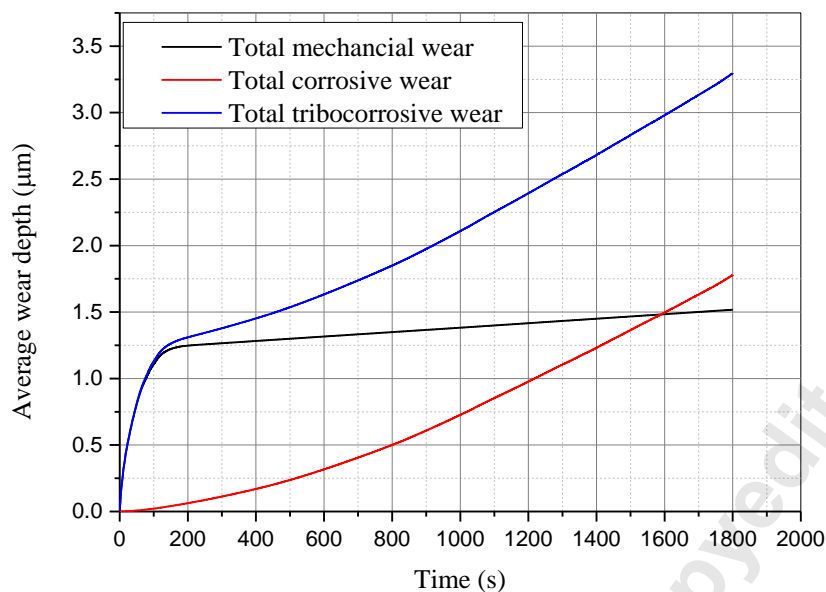


Figure 11 Comparison between total mechanical and total corrosive wear for applied load of 10 N in tribocorrosion condition

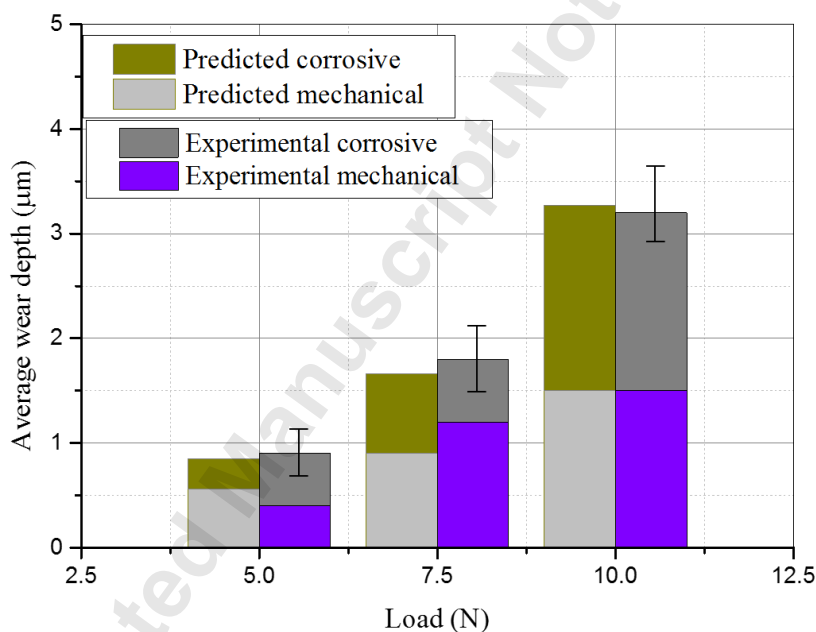


Figure 12 Total average wear depth and the contributions of mechanical and corrosive wear components

5.1.3 Synergism effects

As explained in the previous section, the mechanical wear calculated via the model is the total mechanical wear of the system. The surface topography is being modified by both mechanical and corrosive wear. The resulting mechanical wear calculated by Archard's equation then considers both the pure mechanical wear and the corrosion enhance wear. If the effect of corrosive wear is switched off in the model and the topography is only modified by the

mechanical wear, the component of the pure mechanical wear will be calculated. The pure mechanical wear was then calculated for all the applied loads and the evolution has been plotted in Figure 13 for the case of 10 N. The difference with the total mechanical wear presents the component of the corrosion enhanced wear. Figure 13 shows that the biggest difference between total mechanical wear and the pure mechanical wear arises from the beginning of the simulations where the high plastic deformations are dominant. It is interesting to see that the corrosion enhanced wear of the system happens mainly due to the high plastic deformations at the initial stages of the rubbing. This is perhaps due to the modifications on the asperities resulted from the corrosive wear and also the dynamic process of growth and removal of the oxide layer which changes the topography of the corroding surface. Although the formation of oxides on surface might change the mechanical properties of the interface, this has not been considered in the current model due to its complexity and lack of experimental evidence. In addition, work hardening of the CoCrMo alloys that has been widely reported in the literature might have an impact on the mechanical wear of the system. In the case of pure mechanical wear (without considering the effect of electrochemistry), the amount of plastic deformation at initial stages is much lower. This shows that the surfaces conform to each other at the initial stages. On the other hand, when the surfaces experience corrosive wear, the asperities of two surfaces do not conform well and high plastic deformations occur. The rate of the steady-state mechanical wear seems not to be affected significantly with the effect of corrosion.

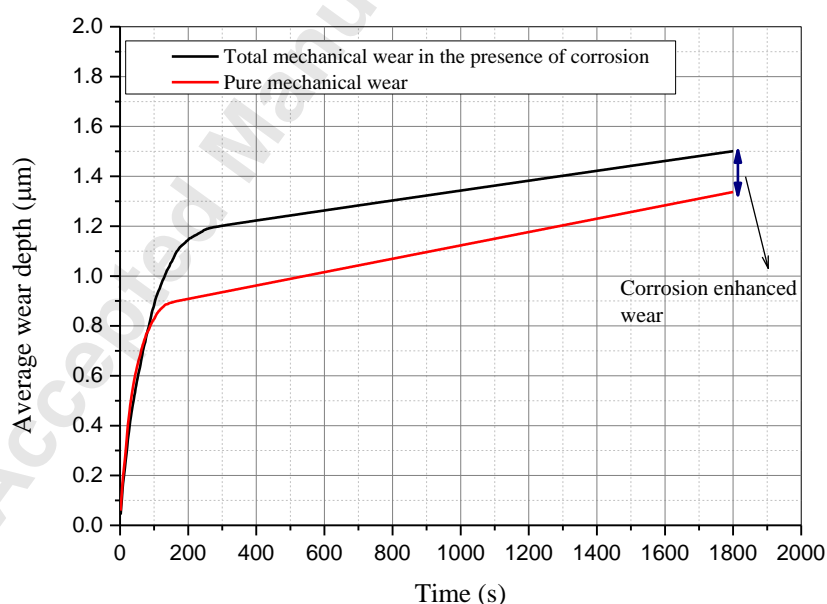


Figure 13 Difference in the total mechanical wear in the presence of the corrosion and the pure mechanical wear in the absence of the corrosion (simulation)

Components of the pure mechanical wear and the corrosion enhanced wear for the applied loads of 5, 7.5 and 10 N have been plotted in Figure 14. It can be noted that the corrosion enhanced wear is a significant part of the total mechanical wear. This is the first time that the synergistic effect of corrosion on the mechanical wear in a tribocorrosive wear environment has been numerically modelled. For comparison purposes, both components of mechanical wear and the component of the corrosive wear have been plotted in Figure 15 to show the contributions of each in the total wear of the system. As the load increases, the contribution of the corrosive wear dominates. In all three applied loads, the corrosion enhanced wear is higher than the pure mechanical wear which shows the significance of the synergistic effects in a tribocorrosive wear system.

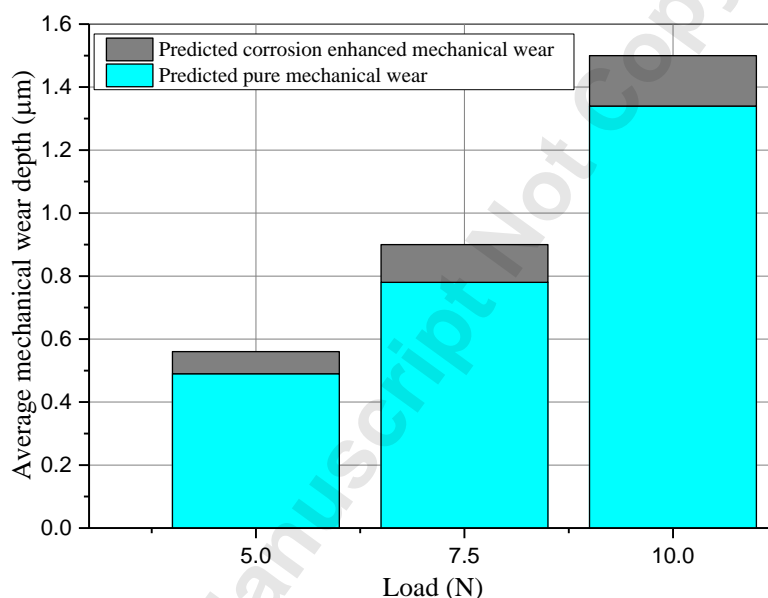


Figure 14 Components of pure mechanical wear and the corrosion enhanced mechanical wear of the total mechanical wear (simulation)

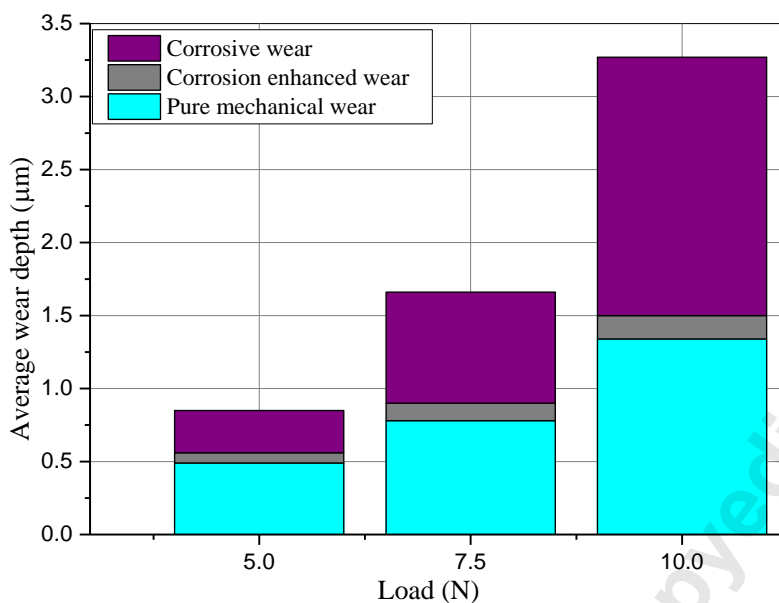


Figure 15 Different components of the total tribocorrosive wear for applied loads of 5, 7.5 and 10 N (simulation)

5.2 Effect of load on synergistic effects

The mechanistic model of the tribocorrosion is known to consider all the possible mechanical and chemical interactions as the following:

$$V_T = V_m + V_c + \Delta V_{cw} + \Delta V_{wc} \quad (9)$$

in which, V_T is the total tribocorrosive wear and V_m and V_c are the material loss due to pure mechanical wear and pure corrosive wear, respectively. Terms ΔV_{cw} and ΔV_{wc} stand for the corrosion-enhanced wear and the wear-enhanced corrosion, respectively. In this paper, the calculation of the pure mechanical wear and the corrosion enhanced mechanical wear has been shown in the previous section for the first time. In this section, the effect of applied load on the components of the tribocorrosive wear is reported. Simulations were carried out at different loads and the values for total tribocorrosive wear, total mechanical wear, total corrosive wear, pure mechanical wear and corrosion enhanced wear has been obtained.

Figure 16 represents the total mechanical and corrosive wear depth for different applied loads ranging from 1 to 20 N. The results show an increase in both corrosive and mechanical wear. However, the rate of increase for the corrosive wear seems to be faster. For this reason, the corrosive wear depth was plotted vs the mechanical wear depth at different loads and the results are plotted in Figure 17. The results show that the corrosive wear increases linearly with the

value of the mechanical wear. It was reported by Cao et al [37] that the total mechanical wear is proportional to $F^{1.3129}$ and total corrosive (chemical) wear is proportional to $F^{0.6565}$ in which F is the applied load. These power constants were obtained by considering the share of load and the lubrication severity in a mixed lubrication regime. The simulation results of this paper have been fitted to the linear model as well as the models proposed by Cao. The results are plotted in Figure 18 for mechanical wear and Figure 19 for the corrosive wear respectively. Both fitting models can be used to capture the effect of load on the mechanical and corrosive wear. However there are slight differences in the trends of the models especially for the corrosive wear. This can be due to the difference in the nature of the models. The numerical model of this work incorporates a deterministic contact mechanics model and does not consider a mixed lubrication model and the lubrication properties however Cao's model is developed for a mixed lubrication regime. In addition, for corrosive wear, Cao showed the dependence of corrosive wear to $\frac{1}{H^{0.5}}$. The hardness value in our work is constant during the simulation which can be another reason for the discrepancy of the simulation data and the fit. Therefore for the current model, the simulation results of the corrosive and mechanical wear were fit with a linear model. This seems to be a good assumption in the boundary lubrication regime. Similar results were also reported by Zugelj et al. [36] where they experimentally showed a linear increase of the real area of contact with the applied load.

The pure mechanical wear (V_m) and the corrosion enhanced mechanical wear (ΔV_{cw}) components of the total tribocorrosive wear are calculated based on the procedure in Section 5.1.3 and the results are plotted in Figure 20 for different values of the applied load. The results demonstrate that both components of the mechanical wear linearly increase with the applied load. This is well-known for the case of pure mechanical wear which is following the Archard wear law and the slope of the line should be proportional to the coefficient of mechanical wear. Interestingly, the corrosion enhanced wear is also linearly increasing with the applied load with a higher rate than the pure mechanical wear. The reason for this is the increased value of the corrosive wear with the load and therefore increase in the topography evolution share of the electrochemistry. While the topography is evolved with the electrochemistry this will in turn affect the plastic deformations (see Section 5.1.3). Hence, the increase in the corrosive wear will increase the corrosion enhanced wear component as well.

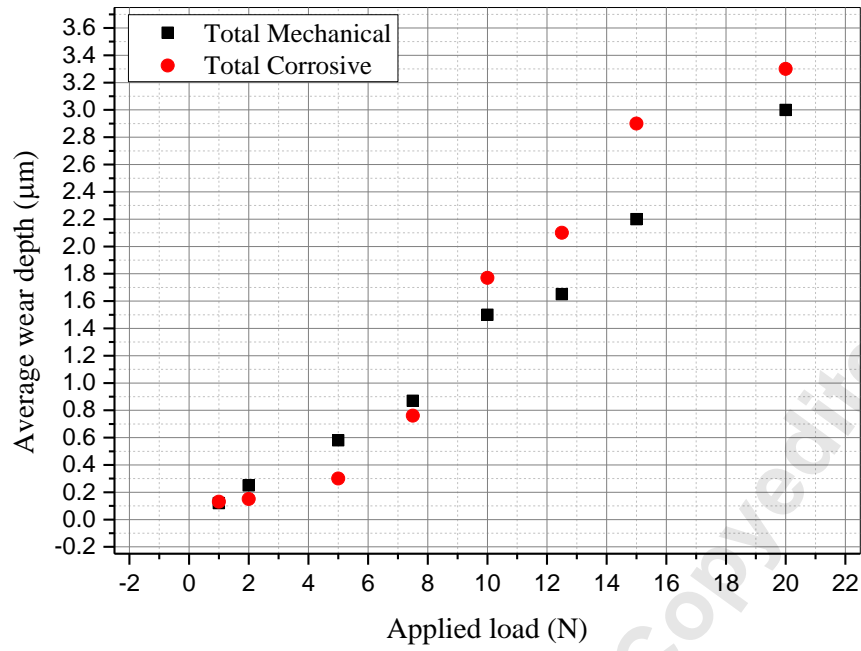


Figure 16 The total mechanical and corrosive wear depth at different applied loads; simulations

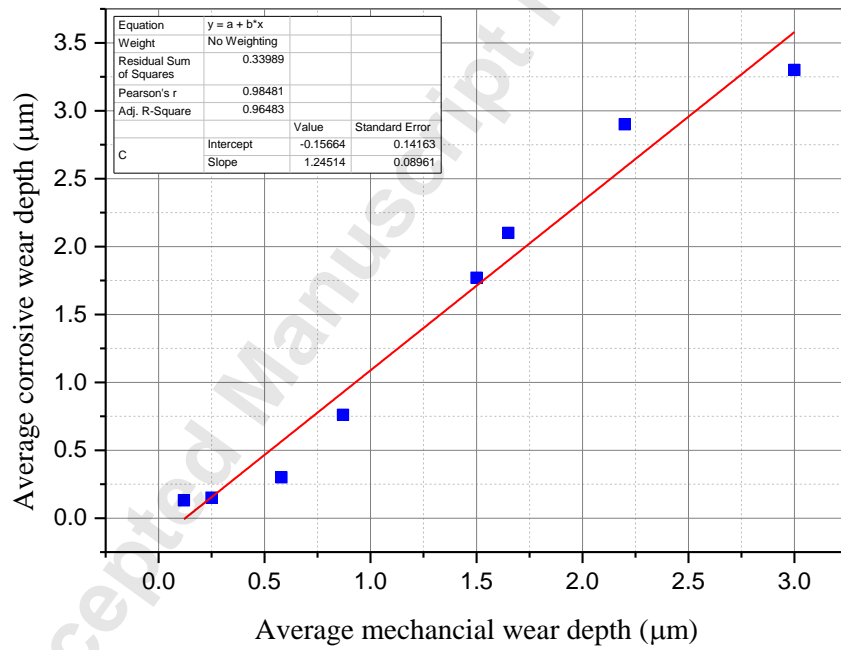


Figure 17 Variations of the corrosive wear with the mechanical wear; simulations

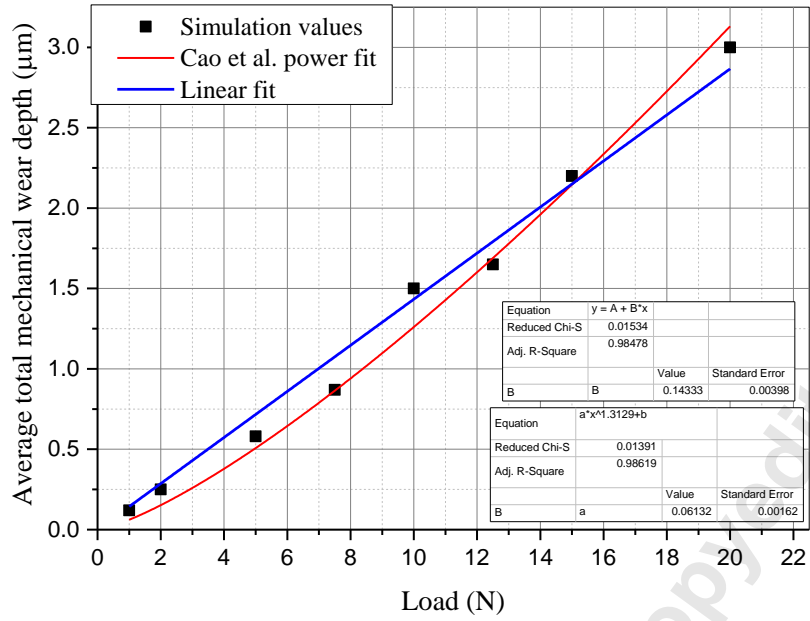


Figure 18 Comparison of the model proposed by Cao et al [37] and the linear fit; Total mechanical wear

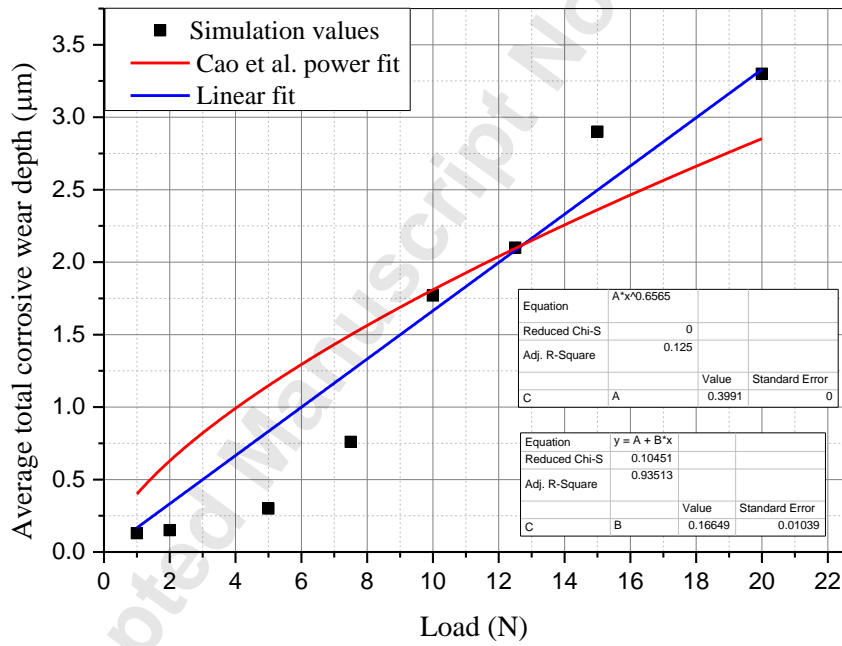


Figure 19 Comparison of the model proposed by Cao et al [37] and the linear fit; total electrochemical wear

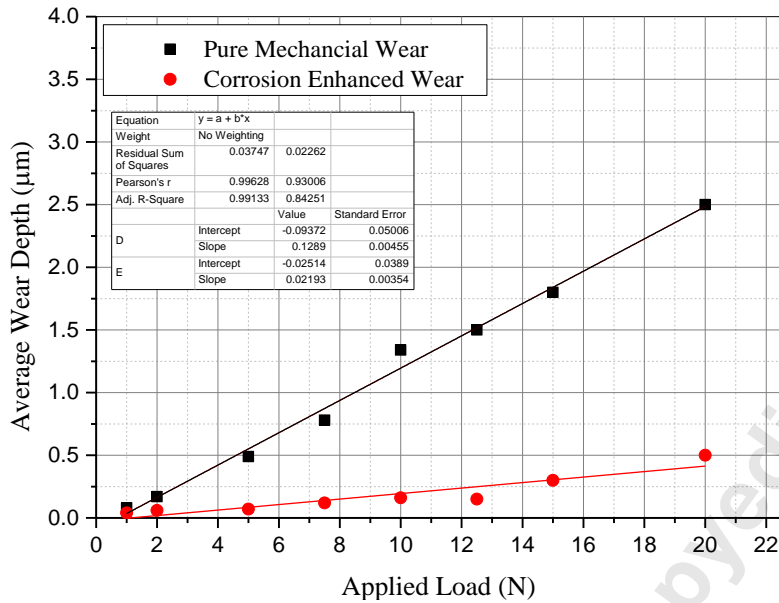


Figure 20 Variation of the pure mechanical wear and the corrosion enhanced wear with the applied load; simulation results

The results explained above show that all components of the tribocorrosive wear linearly vary with load. This suggests that the overall tribocorrosive wear can be modelled mechanistically as the following:

$$W_T = (\alpha_m + \alpha_c + \alpha_{mc} + \alpha_{cm}) \cdot \frac{L}{H} \cdot s \quad (10)$$

In which W_T is the total tribocorrosive wear (m^3), α_m is the pure mechanical wear rate, α_c is the pure corrosive wear rate, α_{mc} is the wear enhanced corrosion wear rate, α_{cm} is the corrosion enhanced wear rate, L is the applied load (N), H is the hardness (N/m^2) and s is the sliding distance (m). The total tribocorrosive wear can be mechanistically modelled using an Archard-type wear model but considering different wear rates for different components. This is an interesting finding. Archard introduced the linear dependency of the wear volume on the applied load. He did not distinguish between different modes and mechanisms of the wear. In the current paper, results have shown that simple Archard-type wear models are universal and can accommodate different components of a tribocorrosive material degradation too. The model of Equation 10 is principally redefining Archard's wear law and including pure mechanical wear, wear enhanced corrosion and corrosion enhanced wear and is not proposing a new concept. One simplicity in introducing the current model is the linear dependency of the wear on the sliding distance which results clearly show a different scenario. Perhaps it is a reasonable assumption in the steady-state wear mode. However this is well-accepted and

Archard-type wear models are widely used in the literature despite the importance of the running-in period. The model of Equation 10 can be used as a new conceptual mechanistic model of tribocorrosion. It is reasonable to have an Archard-type model for the pure mechanical wear but the results have shown that corrosion enhanced wear and the corrosive wear also change linearly with the load but with a different wear rate.

6 Limitations of the current approach

The model presented here incorporates a novel approach to model the tribocorrosion phenomena by taking into account the corrosive and mechanical wear simultaneously at the asperity level. This will lead to a unique capability to directly calculate different components of a tribocorrosive wear. However, based on the nature of the model, it lacks certain physics of the real tribocorrosion system. In order to highlight the model simplifications and give directions for the future studies in this area, the specific model limitations are listed as the following:

- Consideration of tribocorrosion at the free corrosion potential (E_{corr}) of the alloy. This will lead to realistic current measurements and realistic contribution of corrosion in the total tribocorrosive wear.
- The share of current going into the solution and its effect on the growth of the oxide layer and the consequent electrochemical calculations.
- The model has been validated against 3 different values of normal load and the simulated wear results for other loads has been compared with the work of Cao et al. [37]. Although the simulation results show good agreement, more experiments will be conducted in the future for the sake of model validation in a wider range of loads and lubrication conditions.
- The importance of oxide layer effects on the mechanical properties of the contacting surfaces; i.e. the mechanical properties of the oxide layer itself.
- Work hardening of the alloys that face tribological contacts and the evolution of their mechanical properties with respect to flash temperature, pressure etc.
- The tribochemistry of the corrosive lubricant and the surfaces that might change the mechanical, chemical and physical properties of the interface.
- The properties of the lubricant has not been considered in this model. Therefore the model is not a mixed lubrication model and is solely a boundary contact model. It will be interesting to see the effect of different loading severities and lubrication regimes on

the tribocorrosive wear. Development of the mixed lubrication tribocorrosion model is the ongoing research of the authors.

- Consideration of the more complex wear phenomena than the simple adhesive wear that is described by Archard. Since the properties of the interface and the adherence of the oxide layer is dependent on several parameters such as void formation and coalescence, dislocation mobility and annihilation which can all result in different stress fields in the material [38]. Therefore complex mechanical and microstructural changes might occur in the contacting body that result in very complex mechanical wear modes.

7 Conclusions

A tribocorrosion model is developed that incorporates already established electrochemistry model and Archard's type mechanical model on asperity scale. The mechanical wear and corrosion predicted by the model have been validated with reciprocating tribocorrosion experiments with CoCrMo plate in contact with Si_3N_4 ball. The following findings can be highlighted:

- In contrast to the mechanical wear, the total corrosive wear shows a different pattern with an increasing rate with time. The accumulative corrosive wear increases with time because the real area of contact increases as the surfaces wear out.
- The results suggest that the total corrosive wear linearly increase with the total mechanical wear. This can be due to the linear increase of the real area of contact with the mechanical wear.
- Both pure mechanical and corrosion enhanced wear of the system linearly increase with the applied load.
- Corrosion-enhanced wear was modelled for the first time. Linear increase of the corrosion enhanced wear can be due to the linear increase of the total corrosive wear and the corresponding topography variations.
- More credit should be given to the well-known Archard's wear law. Archard's wear model can accommodate complicated modes of wear such as tribocorrosive wear (where corrosion and mechanical wear are promoting each other) without taking care of individual components. Linear assumption of Archard is also reflected in the trends seen in this paper.

References

- [1] Wood, R. J., 2007, "Tribo-corrosion of coatings: a review," *Journal of Physics D: Applied Physics*, 40(18), p. 5502.
- [2] Watson, S., Friedersdorf, F., Madsen, B., and Cramer, S., 1995, "Methods of measuring wear-corrosion synergism," *Wear*, 181, pp. 476-484.
- [3] Watson, S., Madsen, B., and Cramer, S., 1995, "Wear-corrosion study of white cast irons," *Wear*, 181, pp. 469-475.
- [4] Jiang, X., Li, S., Tao, D., and Yang, J., 1993, "Accelerative effect of wear on corrosion of high-alloy stainless steel," *Corrosion*, 49(10), pp. 836-841.
- [5] Barker, K., and Ball, A., 1989, "Synergistic abrasive—corrosive wear of chromium containing steels," *British Corrosion Journal*, 24(3), pp. 222-228.
- [6] De Souza, V., and Neville, A., 2003, "Corrosion and erosion damage mechanisms during erosion—corrosion of WC—Co—Cr cermet coatings," *Wear*, 255(1), pp. 146-156.
- [7] Jiang, J., Stack, M., and Neville, A., 2002, "Modelling the tribo-corrosion interaction in aqueous sliding conditions," *Tribology International*, 35(10), pp. 669-679.
- [8] Landolt, D., and Mischler, S., 2011, *Tribocorrosion of passive metals and coatings*, Elsevier.
- [9] Mischler, S., Debaud, S., and Landolt, D., 1998, "Wear-accelerated corrosion of passive metals in tribocorrosion systems," *Journal of the Electrochemical Society*, 145(3), pp. 750-758.
- [10] Landolt, D., Mischler, S., and Stemp, M., 2001, "Electrochemical methods in tribocorrosion: a critical appraisal," *Electrochimica Acta*, 46(24), pp. 3913-3929.
- [11] Mischler, S., and Muñoz, A. I., 2013, "Wear of CoCrMo alloys used in metal-on-metal hip joints: a tribocorrosion appraisal," *Wear*, 297(1), pp. 1081-1094.
- [12] Stemp, M., Mischler, S., and Landolt, D., 2003, "The effect of mechanical and electrochemical parameters on the tribocorrosion rate of stainless steel in sulphuric acid," *Wear*, 255(1), pp. 466-475.
- [13] Jemmely, P., Mischler, S., and Landolt, D., 2000, "Electrochemical modeling of passivation phenomena in tribocorrosion," *Wear*, 237(1), pp. 63-76.
- [14] Olsson, C.-O., and Stemp, M., 2004, "Modelling the transient current from two rubbing electrode configurations: insulating pin on metal substrate and metal pin on insulating substrate," *Electrochimica acta*, 49(13), pp. 2145-2154.
- [15] Ghanbarzadeh, A., Piras, E., Nedelcu, I., Brizmer, V., Wilson, M. C. T., Morina, A., Dowson, D., and Neville, A., 2016, "Zinc Dialkyl Dithiophosphate Antiwear Tribofilm and its Effect on the Topography Evolution of Surfaces: A Numerical and Experimental Study," *Wear*, 362-363, pp. 186-198.
- [16] Stachowiak, A., and Zwierzycki, W., 2012, "Analysis of the tribocorrosion mechanisms in a pin-on-plate combination on the example of AISI304 steel," *Wear*, 294, pp. 277-285.
- [17] Stachowiak, A., and Zwierzycki, W., 2011, "Tribocorrosion modeling of stainless steel in a sliding pair of pin-on-plate type," *Tribology International*, 44(10), pp. 1216-1224.
- [18] Stachowiak, A., Tyczewski, P., and Zwierzycki, W., 2016, "The application of wear maps for analyzing the results of research into tribocorrosion," *Wear*, 352, pp. 146-154.
- [19] Ghanbarzadeh, A., Salehi, F. M., Bryant, M., and Neville, A., 2017, "Modelling the Evolution of Electrochemistry in a Tribocorrosive Wear Environment," *Tribology International*, submitted.
- [20] Dearnley, P., 2016, *Introduction to Surface Engineering*, Cambridge University Press.
- [21] Ettienne-Modeste, G. A., and Topoleski, L. T., 2013, "Nanomechanical and Wear Behavior of Microtextured Carbide-Coated CoCrMo Alloy Surfaces," *Journal of Tribology*, 135(4), p. 041301.
- [22] Dearnley, P., 1999, "A review of metallic, ceramic and surface-treated metals used for bearing surfaces in human joint replacements," *Proceedings of the Institution of Mechanical Engineers, Part H: Journal of Engineering in Medicine*, 213(2), pp. 107-135.

- [23] Li, D., Guruvenket, S., Azzi, M., Szpunar, J., Klemberg-Sapieha, J., and Martinu, L., 2010, "Corrosion and tribo-corrosion behavior of a-SiC x: H, a-SiN x: H and a-SiC x N y: H coatings on SS301 substrate," *Surface and Coatings Technology*, 204(9), pp. 1616-1622.
- [24] Li, D., Guruvenket, S., and Klemberg-Sapieha, J. E., 2011, "Corrosion and tribo-corrosion enhancement of SS301 and Ti-6Al-4V substrates by amorphous hydrogenated SiN/SiC/aC multilayer coating architecture," *Surface and Coatings Technology*, 206(7), pp. 1893-1898.
- [25] Beadling, A., Bryant, M., Dowson, D., and Neville, A., "The effect of microseparation on corrosion rates of metal-on-metal total hip replacements," *NACE International*.
- [26] Beadling, A. R., Bryant, M., Dowson, D., and Neville, A., 2016, "Tribocorrosion of hard-on-hard total hip replacements with metal and ceramic counterfaces under standard and adverse loading conditions," *Tribology International*, 103, pp. 359-367.
- [27] Xuefeng Tian, B. B., 1996, "A Numerical Three-Dimensional Model for the Contact of Rough Surfaces by Variational Principle."
- [28] Hu, Y., and Tonder, K., 1992, "Simulation of 3-D random rough surface by 2-D digital filter and Fourier analysis," *International Journal of Machine Tools and Manufacture*, 32(1), pp. 83-90.
- [29] Ghanbarzadeh, A., Wilson, M., Morina, A., Dowson, D., and Neville, A., 2016, "Development of a New Mechano-Chemical Model in Boundary Lubrication," *Tribology International*, 93, pp. 573-582.
- [30] Vetter, K., and Gorn, F., 1973, "Kinetics of layer formation and corrosion processes of passive iron in acid solutions," *Electrochimica Acta*, 18(4), pp. 321-326.
- [31] J. Andersson, A. A., R. Larsson, 2011, "Numerical simulation of a wear experiment," *Wear*, 271(11), pp. 2947-2952.
- [32] Morales-Espejel, G., Brizmer, V., and Piras, E., 2015, "Roughness evolution in mixed lubrication condition due to mild wear," *Proceedings of the Institution of Mechanical Engineers, Part J: Journal of Engineering Tribology*, p. 1350650115577404.
- [33] Morales-Espejel, G. E., and Brizmer, V., 2011, "Micropitting modelling in rolling-sliding contacts: Application to rolling bearings," *tribology transactions*, 54(4), pp. 625-643.
- [34] Mischler, S., 2008, "Triboelectrochemical techniques and interpretation methods in tribocorrosion: a comparative evaluation," *Tribology International*, 41(7), pp. 573-583.
- [35] Akonko, S., Li, D., and Ziomek-Moroz, M., 2005, "Effects of cathodic protection on corrosive wear of 304 stainless steel," *Tribology Letters*, 18(3), pp. 405-410.
- [36] Zigelj, B. B., and Kalin, M., 2017, "Submicron-scale experimental and theoretical analyses of multi-asperity contacts with different roughnesses," *Tribology International*.
- [37] Cao, S., Maldonado, S. G., and Mischler, S., 2015, "Tribocorrosion of passive metals in the mixed lubrication regime: theoretical model and application to metal-on-metal artificial hip joints," *Wear*, 324, pp. 55-63.
- [38] Guadalupe, S., Cao, S., Cantoni, M., Chitty, W.-J., Falcand, C., and Mischler, S., 2017, "Applicability of a recently proposed tribocorrosion model to CoCr alloys with different carbides content," *Wear*, 376, pp. 203-211.

List of Figures

Figure 1 Schematic of tribometer and the three-electrode cell used for electrochemical measurement

Figure 2 Evolution of the current density as a function of time for 3 applied loads of 5, 7.5 and 10 N

Figure 3 2D microscopic images of the plate wear scars after reciprocating tribometer testing under various loads of (a) 5N (b) 7.5N (c) 10N

Figure 4 Wear scar depth for CoCrMo samples during reciprocating tribometer testing with varying load

Figure 5 Movement of the surfaces and exposure of the nascent surface asperities to the corrosive environment

Figure 6 Flowchart of the whole numerical approach for calculation of the electrochemistry in tribocorrosion conditions

Figure 7 Sensitivity of the corrosion model to the calibration parameter ($igrowth_0$)

Figure 8 Sensitivity of the model to the non-dimensional coefficient of mechanical wear

Figure 9 Average mechanical wear depth evolution for applied loads of 5, 7.5 and 10 N from simulations in tribocorrosion condition

Figure 10 Average corrosive wear depth evolution for applied loads of 5, 7.5 and 10 N from simulation in tribocorrosion condition

Figure 11 Comparison between total mechanical and total corrosive wear for applied load of 10 N in tribocorrosion condition

Figure 12 Total average wear depth and the contributions of mechanical and corrosive wear components

Figure 13 Difference in the total mechanical wear in the presence of the corrosion and the pure mechanical wear in the absence of the corrosion (simulation)

Figure 14 Components of pure mechanical wear and the corrosion enhanced mechanical wear of the total mechanical wear (simulation)

Figure 15 Different components of the total tribocorrosive wear for applied loads of 5, 7.5 and 10 N (simulation)

Figure 16 The total mechanical and corrosive wear depth at different applied loads; simulations

Figure 17 Variations of the corrosive wear with the mechanical wear; simulations

Figure 18 Comparison of the model proposed by Cao et al [37] and the linear fit; Total mechanical wear

Figure 19 Comparison of the model proposed by Cao et al [37] and the linear fit; total electrochemical wear

Figure 20 Variation of the pure mechanical wear and the corrosion enhanced wear with the applied load; simulation results

List of Tables

Table 1 Properties of the samples used in the experiments

Table 2 Tribocorrosion test parameters used in this study

Table 3 Chemical composition of the CoCrMo plate

Table 4 Fitting parameters in the electrochemistry model

Table 5 Calibrated dimensionless coefficient of mechanical wear

Accepted Manuscript Not Copyedited

